



# $Q^{(n)}$ -Species Distribution in $K_2O \cdot 2 SiO_2$ Glass by $^{29}Si$ Magic Angle Flipping NMR

Michael C. Davis,<sup>†</sup> Derrick C. Kaseman,<sup>†</sup> Sahar M. Parvani,<sup>†</sup> Kevin J. Sanders,<sup>†</sup>  
 Philip J. Grandinetti,<sup>\*,†</sup> Dominique Massiot,<sup>‡</sup> and Pierre Florian<sup>‡</sup>

*Department of Chemistry, The Ohio State University, 120 W. 18<sup>th</sup> Avenue, Columbus, Ohio 43210-1173, and CNRS, UPR3079 CEMHTI, 1D Avenue de la Recherche Scientifique, 45071 Orléans Cedex 2, France, and Universite d Orleans, Avenue du Parc Floral, BP 6749, 45067 Orleans Cedex 2, France*

E-mail: grandinetti.org/Contact

## Abstract

Two-dimensional magic angle flipping (MAF) was employed to measure the  $Q^{(n)}$  distribution in a  $^{29}Si$  enriched potassium disilicate glass ( $K_2O \cdot 2 SiO_2$ ). Relative concentrations of  $[Q^{(4)}] = 7.2\% \pm 0.3\%$ ,  $[Q^{(3)}] = 82.9\% \pm 0.1\%$ ,  $[Q^{(2)}] = 9.8\% \pm 0.6\%$  were obtained. Using the thermodynamic model for  $Q^{(n)}$  species disproportionation these relative concentrations yield an equilibrium constant  $k_3 = 0.0103 \pm 0.0008$ , indicating, as expected, that the  $Q^{(n)}$  species distribution is close to binary in the potassium disilicate glass. A Gaussian distribution of isotropic chemical shifts was observed for each  $Q^{(n)}$  species with mean values of  $-82.74 \pm 0.03$  ppm,  $-91.32 \pm 0.01$  ppm, and  $-101.67 \pm 0.02$ , and standard deviations of  $3.27 \pm 0.03$  ppm,  $4.19 \pm 0.01$  ppm, and  $5.09 \pm 0.03$  for  $Q^{(2)}$ ,  $Q^{(3)}$ , and  $Q^{(4)}$ , respectively. Additionally, nuclear shielding anisotropy values of  $\zeta = -85.0 \pm 1.3$  ppm,  $\eta = 0.48 \pm 0.02$  for  $Q^{(2)}$ , and  $\zeta = -74.9 \pm 0.2$  ppm,  $\eta = 0.03 \pm 0.01$  for  $Q^{(3)}$  were observed in the potassium disilicate glass.

\*To whom correspondence should be addressed

<sup>†</sup>OSU

<sup>‡</sup>CNRS

## Introduction

Non-crystalline materials have the advantage that their properties are isotropic and vary continuously with the composition so any value of a particular property, within limits, can be obtained by adjusting the composition.<sup>1,2</sup> Unfortunately, for many non-crystalline materials, a lack of sound theoretical models relating composition and structure to properties makes their design and preparation difficult. In non-crystalline silicates the relative abundance of anionic species are essential part of any structure-based model and one of the most fundamental aspects of this speciation is the distribution of silicate tetrahedra with varying numbers ( $n$ ) of bridging oxygen, commonly described as  $Q^{(n)}$  species. In earlier work<sup>3,4</sup> we showed that an NMR method such as Magic-Angle Flipping (MAF),<sup>5,6</sup> which produces a two dimensional (2D) spectrum correlating isotropic and anisotropic nuclear shielding contributions to the solid-state spectrum, can be used to give over an order of magnitude improvement in quantifying  $Q^{(n)}$  species concentrations when compared to conventional  $^{29}Si$  Magic-Angle Spinning (MAS) lineshape analysis. Additionally, this method does not require the assumption of a Gaussian distribution of isotropic  $^{29}Si$  chemical shifts for the different  $Q^{(n)}$  species. Its accuracy and precision in quantifying  $Q^{(n)}$  were demonstrated in a well-understood sodium silicate glass binary composi-

tion<sup>3</sup>. The results were used in a thermodynamic disproportionation model to calculate the equilibrium constant for  $Q^{(3)}$  ( $k_3 = 0.0129 \pm 0.0001$ ). The same approach was applied successfully on a  $\text{CaO} \cdot \text{SiO}_2$  glass,<sup>4</sup> which has a completely unresolved  $^{29}\text{Si}$  MAS spectrum, to obtain the equilibrium constants  $k_1 = 0.10 \pm 0.02$ ,  $k_2 = 0.156 \pm 0.005$ , and  $k_3 = 0.11 \pm 0.02$  for the disproportionation reactions in  $\text{CaO} \cdot \text{SiO}_2$ . These latter results were the first quantitative measure of  $Q^{(n)}$  distributions in the alkaline earth silicate glass, and indicated a significantly greater deviation from a binary model of  $Q^{(n)}$  species disproportionation in alkaline earth silicate melts compared to alkali silicate melts.

Since 2D MAF requires a solid-state NMR probe with specialized hardware to reorient the sample rotation axis, it should also be noted that there are a number of alternative solid-state methods including magic angle hopping (MAH), magic angle turning (MAT), and phase adjusted spinning sidebands (PASS) for obtaining the same 2D correlation of isotropic and anisotropic nuclear shielding contributions,<sup>7-11</sup> some of which have also been applied to glasses.<sup>12-17</sup> While these other methods have been used to obtain more qualitative analyses of  $Q^{(n)}$  species in silicate glasses only MAF, so far, has been successfully applied in improving  $Q^{(n)}$  quantification in silicate glasses. In addition to improved quantification of  $Q^{(n)}$  species, 2D double-quantum NMR techniques have also been used to establish connectivities between  $Q^{(n)}$  species by exploiting dipolar couplings<sup>18-21</sup> and more recently through  $J$  couplings.<sup>22-24</sup> These experiments have also provided more accurate mean chemical shifts for  $Q^{(n)}$  sites to aid in deconvolution of overlapping Gaussian lineshapes in MAS spectra.

Recently, Florian and coworkers<sup>24</sup> found, through *ab initio* calculations calibrated with experimental measurements in crystalline phases, a close-to-linear relationship between the  $^2J_{\text{Si-O-Si}}$  coupling and the Si–O–Si bond angle. Additionally, they measured a 2D  $J$ -resolved MAS spectrum, which correlates  $^{29}\text{Si}$  isotropic chemical shifts and  $^2J_{\text{Si-O-Si}}$  couplings, for a  $^{29}\text{Si}$ -enriched  $\text{CaO} \cdot \text{SiO}_2$  glass. Generally, the intensity in a  $^{29}\text{Si}$  MAS lineshape of a fully  $^{29}\text{Si}$ -enriched silicate glass at a given isotropic chemical shift can

contain contributions from any of the  $Q^{(n)}$  sites, and a  $^{29}\text{Si}$  nucleus in a given  $Q^{(n)}$  will experience  $n$  different  $^2J_{\text{Si-O-Si}}$  couplings. Thus, critical in the analysis of the 2D  $J$ -resolved MAS spectrum of  $\text{CaO} \cdot \text{SiO}_2$  glass were the  $^{29}\text{Si}$  chemical shift distributions for the five  $Q^{(n)}$  populations in  $\text{CaO} \cdot \text{SiO}_2$  glass derived from the  $^{29}\text{Si}$  2D MAF spectrum of Zhang et al.<sup>4</sup> That is, knowledge of these five  $Q^{(n)}$  isotropic chemical shift distributions allowed Florian and coworkers to fit each  $J$ -resolved cross section to the appropriate number of  $J$  couplings, and use their relationship between the  $^2J_{\text{Si-O-Si}}$  coupling and the Si–O–Si bond angle to determine the Si–O–Si bond angles associated with  $Q^{(3)}$ ,  $Q^{(2)}$ , and  $Q^{(1)}$  sites in a silicate glass for the first time.

Here we present the first of a multi-part solid-state NMR study on a potassium disilicate glass to (1) determine the its distribution of NMR parameters, (2) establish relationships between NMR parameters and local structure, and (3) map measured NMR parameters distributions into structural distributions. The focus of this work is the measurement of the distribution of  $^{29}\text{Si}$  nuclear shielding tensors in a  $^{29}\text{Si}$ -enriched potassium disilicate glass and interpretation in terms of the structures, specifically  $Q^{(n)}$  species, present in the glass. Since the  $^{29}\text{Si}$  MAS spectrum of  $\text{K}_2\text{O} \cdot 2 \text{SiO}_2$  is completely unresolved, a simple deconvolution of the  $^{29}\text{Si}$  MAS lineshape is not possible without additional assumptions to constrain the least-squares fit.<sup>23</sup> With MAF we avoid such assumptions and obtain not only the distribution of  $^{29}\text{Si}$  isotropic chemical shifts for each  $Q^{(n)}$  but also the distribution of principal components of the  $^{29}\text{Si}$  nuclear shielding tensor in the glass. Although less studied than the isotropic chemical shift, the  $^{29}\text{Si}$  nuclear shielding tensor can not only provide a more reliable identification of  $Q^{(n)}$  species, but also probe structural differences within the first coordination sphere around silicon in a given  $Q^{(n)}$  environment.<sup>25-28</sup> Thus, in addition to quantifying  $Q^{(n)}$  species, another objective of this study is to obtain accurate nuclear shielding tensor parameters for further refinement of these structure relationships. Future work on this potassium disilicate composition will focus on examining correlations between  $^2J_{\text{Si-O-Si}}$  couplings and  $^{29}\text{Si}$  nuclear shielding tensors, and exploring

their potential as probes of structure in silicate glasses.

## Experimental

### Sample Preparation

Approximately 450 mg of sample were synthesized from high purity  $\text{K}_2\text{CO}_3$  (Aldrich, 99+%) and 96.74%  $^{29}\text{Si}$  enriched  $\text{SiO}_2$  (CortecNet). Before synthesis the  $\text{SiO}_2$  was heat treated at  $600^\circ\text{C}$  for 5 hours in order to remove protons present in the sample, and was then kept and handled in an argon-filled glovebox. The starting materials were then decarbonated at  $750^\circ\text{C}$  for three hours, followed by melting for two hours at  $1300^\circ\text{C}$ . The sample was then quenched from this temperature down to room temperature by placing the bottom of the crucible into water. The weight loss during synthesis was within a few percent of nominal. The recovered sample was fully transparent and free of bubbles and was immediately put in an argon-filled glovebox for subsequent grinding. Rotor filling was performed in a argon-filled glove bag. The sealed rotor was then spun using compressed air dried to  $-40^\circ\text{C}$  dewpoint.

### NMR Spectroscopy

Experiments were performed on a hybrid Tecmag Apollo-Chemagnetics CMX II 9.4 Tesla (79.476 MHz for  $^{29}\text{Si}$ ) NMR spectrometer using a modified version of an earlier DAS probe design.<sup>29</sup> All experiments were performed at ambient temperature with a sample spinning rate of 14 kHz. The  $^{29}\text{Si}$  relaxation time was measured using the saturation recovery experiment under MAS condition and  $T_1$  of 89 seconds was measured. A recycle delay of 6 minutes was chosen to prevent saturation. No changes in peak shape as a function of delay time were observed, indicating no differential relaxation among different species. For Bloch decay experiments a radio frequency (rf) strength of 42 kHz was used and 256 complex data points acquired.

The MAF pulse sequence used is shown in Figure 1. This is a shifted-echo<sup>30</sup> version of the MAF experiment,<sup>5,6</sup> where the MAS spectrum is corre-

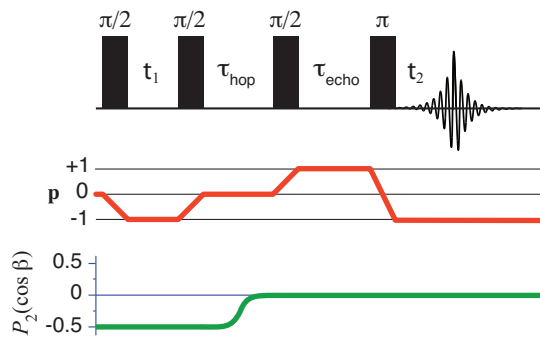


Figure 1: Shifted-echo Magic-Angle Flipping pulse sequence. Here  $t_1$  is the evolution time at  $90^\circ$ ,  $\tau_{\text{hop}}$  is the time to flip the rotor between angles and  $\tau_{\text{echo}}$  is the echo shift.

lated with the spectrum while spinning at perpendicular to the external field. When spinning perpendicular the frequency anisotropies are scaled<sup>31</sup> by a factor of  $-1/2$ . During the MAF experiment the magnetization is stored as Zeeman order during the hop of the rotor axis between angles. The value of  $\tau_{\text{hop}}$  was 80 milliseconds. The echo shift time,  $\tau_{\text{echo}}$  was 2.8 milliseconds. Four dummy scans were performed before starting acquisition to establish a steady state equilibrium and reduce differential relaxation. The number of  $t_1 \times t_2$  points are  $64 \times 128$ , with dwell time of  $62.5\mu\text{s}$  in  $t_1$  and  $t_2$ . Three separate MAF experiments with 32 scans each were performed and coadded. The total number of scans was 96, and the total acquisition time was 25 days. A Gaussian line shape convolution was applied to 2D MAF spectrum with standard deviations of 20 Hz and 100 Hz in the  $\omega_1$  and  $\omega_2$  dimensions, respectively.

In the discussion that follows we will employ the IUPAC definitions for the nuclear shielding and chemical shift interactions.<sup>32</sup> The isotropic nuclear shielding is defined as the trace of the shielding tensor

$$\sigma_{\text{iso}} = \frac{1}{3}(\sigma_{xx} + \sigma_{yy} + \sigma_{zz}), \quad (1)$$

where  $\sigma_{xx}$ ,  $\sigma_{yy}$ , and  $\sigma_{zz}$  are the components of the nuclear shielding tensor in its principal axis system. The isotropic chemical shift,  $\delta_{\text{iso}}$  is defined

$$\delta_{\text{iso}} = (\sigma_{\text{ref}} - \sigma_{\text{iso}})/(1 - \sigma_{\text{ref}}), \quad (2)$$

where  $\sigma_{\text{ref}}$  is the isotropic nuclear shielding of a reference compound, which in this study is TMS. We adopt the Haeberlen convention,<sup>32</sup> where

$$|\sigma_{zz} - \sigma_{\text{iso}}| > |\sigma_{yy} - \sigma_{\text{iso}}| > |\sigma_{xx} - \sigma_{\text{iso}}|, \quad (3)$$

and the shielding anisotropy,  $\zeta$ , and asymmetry parameter,  $\eta$ , are defined as

$$\zeta = \sigma_{zz} - \sigma_{\text{iso}}, \quad (4)$$

and

$$\eta = \frac{\sigma_{yy} - \sigma_{xx}}{\zeta}, \quad (5)$$

respectively.

## Results and Discussion

The one dimensional  $^{29}\text{Si}$  MAS spectrum of  $\text{K}_2\text{O} \cdot 2 \text{SiO}_2$  glass is shown in Figure 2. This spectrum has a broad resonance centered at -93 ppm, consistent with silicon predominately in a  $Q^{(3)}$  coordination. Unlike our earlier study on the alkali silicate glass  $2\text{Na}_2\text{O} \cdot 3 \text{SiO}_2$ , where overlapping but separate  $^{29}\text{Si}$  resonances for  $Q^{(2)}$  and  $Q^{(3)}$  could be observed in the MAS spectrum, there is no clear resolution of  $Q^{(n)}$  species in the MAS spectrum of the  $\text{K}_2\text{O} \cdot 2 \text{SiO}_2$  glass. As noted by Malfait et al.,<sup>23</sup> the skew in the lineshape observed down field indicates  $Q^{(2)}$  sites are present. Although ill posed, we performed a least-squares analysis of the MAS spectrum using three Gaussian lineshape components for a three site model of  $Q^{(2)}$ ,  $Q^{(3)}$ , and  $Q^{(4)}$ . From this analysis we obtained 41.6%, 57.7%, and 0.7% for  $Q^{(2)}$ ,  $Q^{(3)}$ , and  $Q^{(4)}$  populations. Such a result, however, is clearly at odds with the prediction from the charge balance equation,

$$\text{K/Si} = 4[Q^{(0)}] + 3[Q^{(1)}] + 2[Q^{(2)}] + [Q^{(3)}] \quad (6)$$

where our 1D MAS analysis yields a ratio of  $\text{K/Si} = 1.41$  instead of  $\text{K/Si} = 1$  expected for this composition. Analysis of the 1D lineshape therefore indicates that while approximate values for each  $Q^{(n)}$  can be obtained, unconstrained fitting does not provide values that are consistent with the compositional constraints of the sample. As we show (vide infra), utilizing a two dimensional ap-

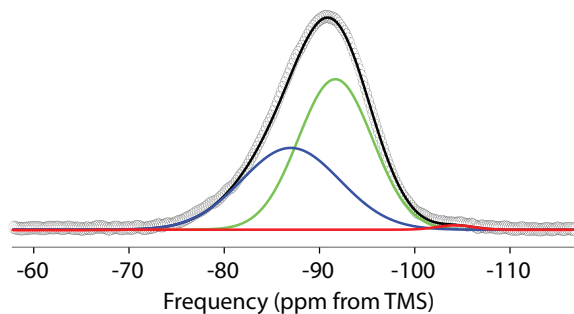


Figure 2: One dimensional  $^{29}\text{Si}$  Magic-Angle Spinning Bloch Decay spectrum of  $\text{K}_2\text{O} \cdot 2 \text{SiO}_2$  glass along with “best-fit” model lineshape and component lineshapes for  $Q^{(4)}$ ,  $Q^{(3)}$ , and  $Q^{(2)}$  resonances. The spectrum baseline was corrected to eliminate any artifacts due to acquisition dead time.

proach such as MAF places additional constraints on the fitting since each cross section is defined by the nuclear shielding parameters ( $\zeta$  and  $\eta$ ) of the  $Q^{(n)}$  site that dominate that particular isotropic chemical shift.

Figure 3 shows the 2D contour plot of the  $^{29}\text{Si}$  MAF spectrum for the  $\text{K}_2\text{O} \cdot 2 \text{SiO}_2$  glass. As illustrated elsewhere<sup>3,4</sup> the five  $Q^{(n)}$  sites have well defined differences in their  $^{29}\text{Si}$  nuclear shielding tensors yielding characteristic anisotropic lineshapes that can distinguish between sites. In Figure 3 one can see from the  $90^\circ$  dimension that the low intensities of the MAS lineshape around -105 ppm are dominated by  $Q^{(4)}$ , the MAS lineshape intensities around -90 ppm are dominated by  $Q^{(3)}$ , and the MAS lineshape intensities around -80 ppm have some contributions from  $Q^{(2)}$ .

The chemical shift anisotropy lineshapes in the individual cross-sections taken parallel to the  $90^\circ$  dimension were least-squares analyzed to obtain the relative contribution of each  $Q^{(n)}$  species to the MAS intensity at the MAS frequency correlated to that cross-section. The anisotropic lineshape for each site was modeled using 5 parameters. These were (1) the isotropic chemical shift position  $\delta_{\text{iso}}$ , (2) the chemical shift tensor anisotropy  $\zeta$ , (3) the chemical shift tensor asymmetry parameter  $\eta$ , (4) the integrated intensity, and (5) a Gaussian line broadening. All sites in each cross-section shared the same isotropic chemical shift and that value was fixed by the isotropic dimen-

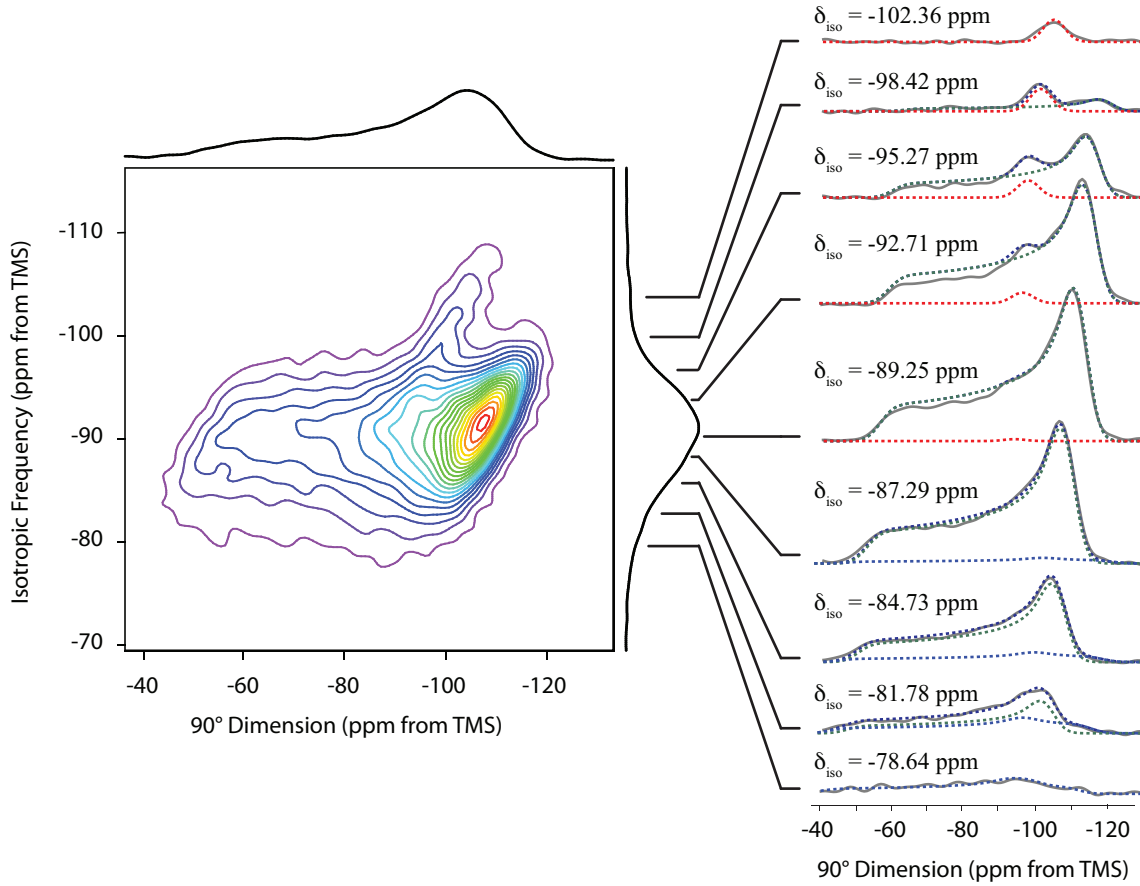


Figure 3: 2D  $^{29}\text{Si}$  MAF NMR spectrum of  $\text{K}_2\text{O} \cdot 2 \text{SiO}_2$  glass (average reduced  $\chi^2 = 2.51$ ). Twenty equally spaced contours are plotted from 5% to 95% of the maximum intensity. One-dimension projections onto the MAS and  $90^\circ$  dimensions are provided and the 1D MAS projection is identical, within the noise level, to the 1D MAS spectrum of Figure 2, indicating that there is no strong  $T_2$  dependence on the MAS lineshape. Selected experimental cross sections (solid lines) are presented with spectral fits (dashed line).

**Table 1: Nuclear shielding anisotropy parameters,  $\zeta$  and  $\eta$ , for  $Q^{(2)}$  and  $Q^{(3)}$  measured in this work for  $\text{K}_2\text{O} \cdot 2 \text{SiO}_2$  compared to previous 2D MAF studies on  $2 \text{Na}_2\text{O} \cdot 3\text{SiO}_2$ ,<sup>3</sup> and on  $\text{CaO} \cdot \text{SiO}_2$ .<sup>4</sup>**

Glass	$\zeta/\text{ppm}$		$\eta$		ref.
	$Q^{(2)}$	$Q^{(3)}$	$Q^{(2)}$	$Q^{(3)}$	
$\text{K}_2\text{O} \cdot 2 \text{SiO}_2$	$-85.0 \pm 1.3$	$-74.9 \pm 0.2$	$0.48 \pm 0.02$	$0.030 \pm 0.006$	this work
$2 \text{Na}_2\text{O} \cdot 3 \text{SiO}_2$	-78	-69	0.53	0.03	3
$\text{CaO} \cdot \text{SiO}_2$	-48.3	-45.4	0.70	0.01	4

sion. In initial least-squares analyses those cross-sections dominated by one  $Q^{(n)}$  species showed little variations in  $\zeta$ ,  $\eta$ , and Gaussian line broadening for the line shape of the dominant species. In cross-sections with strong overlap of  $Q^{(n)}$  species and/or low signal-to-noise the least-squares analyses gave discontinuous unphysical variations in the parameters. Therefore, in performing the final least-squares analysis of each cross-section the nuclear shielding tensor anisotropy  $\zeta$  and asymmetry parameter  $\eta$  for a given  $Q^{(n)}$  site were held fixed at the values obtained when that  $Q^{(n)}$  site was the dominant species in the cross-section. Thus all sites were constrained to have the same optimized Gaussian line broadening of 563 Hz in the  $90^\circ$  dimension, with  $\zeta$  and  $\eta$  fixed at  $\zeta = -85.0 \pm 1.3$  ppm,  $\eta = 0.48 \pm 0.02$  for  $Q^{(2)}$ ,  $\zeta = -74.9 \pm 0.2$  ppm,  $\eta = 0.030 \pm 0.006$  for  $Q^{(3)}$ , and  $\zeta = 0.0$  ppm,  $\eta = 0.0$  for  $Q^{(4)}$ .

The magnitude of  $\zeta$  values for both  $Q^{(2)}$  and  $Q^{(3)}$  are larger than those found in our previous 2D MAF studies on  $2 \text{ Na}_2\text{O} \cdot 3\text{SiO}_2$ ,<sup>3</sup> and  $\text{CaO} \cdot \text{SiO}_2$ <sup>4</sup> glass as shown in Table 1. We find a strong correlation, shown in Figure 4, between the  $\zeta$  for  $Q^{(2)}$  and  $Q^{(3)}$  and the modifier cation potential, calculated using the ionic radii of Whittaker and Muntus.<sup>33</sup> Even after taking into account the possibility of different modifier cation coordination numbers, indicated by roman numerals in Figure 4, the correlation still appears to be relatively linear. This trend is consistent with previous observations by Stebbins.<sup>34</sup> It arises because the silicon–non-bridging oxygen distance increases with increasing modifier cation potential, and as explained by Grimmer and coworkers,<sup>25,26</sup> a longer Si–O distance corresponds to less  $^{29}\text{Si}$  shielding.

Shown in Figure 3 are the 1D projections of the 2D spectrum onto the MAS and  $90^\circ$  dimensions. Additionally, selected  $90^\circ$  dimension cross sections associated with specific isotropic chemical shifts are shown with its “best fit” anisotropic line-shape along with component contributions. From the integrated area of each  $Q^{(n)}$  component line shape in each  $90^\circ$  dimension cross section we construct the distribution of isotropic chemical shifts for each of the  $Q^{(n)}$  resonances, shown in Figure 5. Fitting of the MAF spectrum does not require the distribution of chemical shifts as Gaussian but previous analysis of alkali glasses indi-

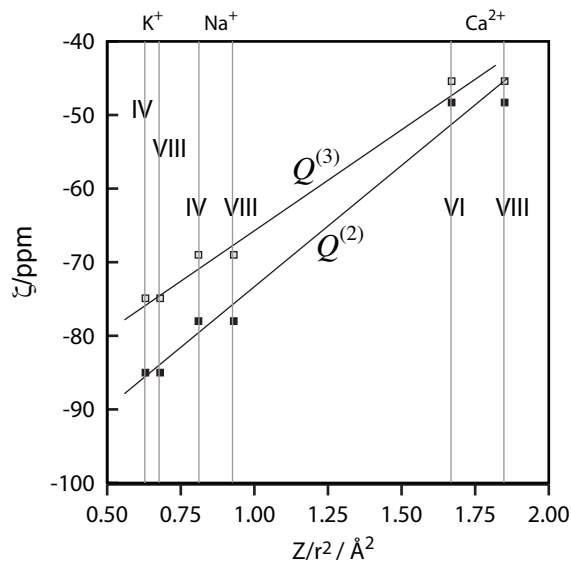


Figure 4: Nuclear shielding anisotropy,  $\zeta$ , for  $Q^{(2)}$  (filled squares) and  $Q^{(3)}$  (open squares) measured using  $^{29}\text{Si}$  2D MAF NMR as a function of network modifier cation potential, with roman numerals indicating different coordination number of modifiers  $X = \text{K}^+$ ,  $\text{Na}^+$ , and  $\text{Ca}^{2+}$ .

cates a Gaussian distribution for each  $Q^{(n)}$  species while a skewed distribution has been observed in alkaline earth glasses where the distribution of  $Q^{(n)}$  is more random. Since the potassium and sodium silicate glasses were expected to be similar and the derived isotropic chemical shifts distributions appear to be approximately Gaussian, the chemical shift distributions for each  $Q^{(n)}$  obtained from the 2D MAF spectrum, including distribution individual intensity uncertainties, were fit to a Gaussian distribution to improve our accuracy in determining the integrated areas and consider intensities otherwise buried in the noise at the edges of the spectrum. The relative concentrations ( $\pm$  one standard deviation) obtained from this analysis are given in Table 2 for the three  $Q^{(n)}$  species. As mentioned earlier, it is important to emphasize that the distribution of the chemical shifts of each  $Q^{(n)}$  species obtained from the 2D MAF analysis are not likely to match that obtained by a least-squares analysis of the 1D MAS spectrum, particularly when the MAS spectrum is unresolved, as was the case in Figure 2.

Our measured MAF-derived populations agree with the expected K/Si ratio of the charge bal-

**Table 2: Gaussian distribution parameters of isotropic chemical shifts of  $Q^{(n)}$ -species in potassium disilicate glass derived from analysis of its 2D  $^{29}\text{Si}$  MAF spectrum.**

Site	Relative Area	Mean Position/ppm	Standard Deviation/ppm
$Q^{(2)}$	$9.8 \pm 0.7\%$	$-82.74 \pm 0.03$	$3.27 \pm 0.03$
$Q^{(3)}$	$83.0 \pm 0.1\%$	$-91.32 \pm 0.01$	$4.19 \pm 0.01$
$Q^{(4)}$	$7.2 \pm 0.3\%$	$-101.67 \pm 0.02$	$5.09 \pm 0.03$

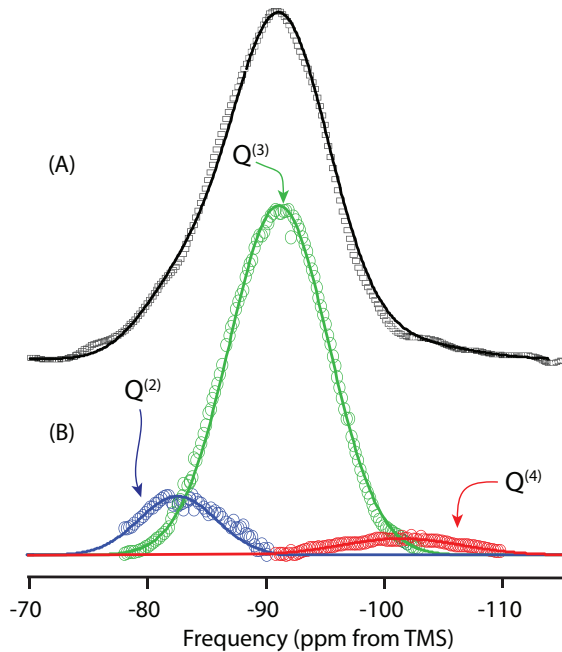


Figure 5:  $^{29}\text{Si}$  NMR MAS results of (a) the isotropic projection of the 2D MAF dataset (squares) with the best fit (dashed line) and (b) and the integrated areas (circles) obtained from the simulated 2D MAF dataset with the Gaussian fits for each sites (solid lines).

ance equation. Each  $Q^{(n)}$  species has a charge of  $-(4-n)$ , which is balanced by the  $+1$  charge of the potassium cations. For this composition the expected K/Si ratio is 1. The K/Si ratio calculated using Eq. (6) and the relative populations in Table 2 is  $1.026 \pm 0.007$ . This value agrees reasonably well with the expected value and offers additional evidence that our measured populations are accurate. The slight deviation from unity is likely due to weight loss during synthesis and thus a slight change in stoichiometry. Some deviation could additionally arise from small defects in the glass network (uncompensated negative charge). The existence of small concentrations of  $Q^{(2)}$  and  $Q^{(3)}$

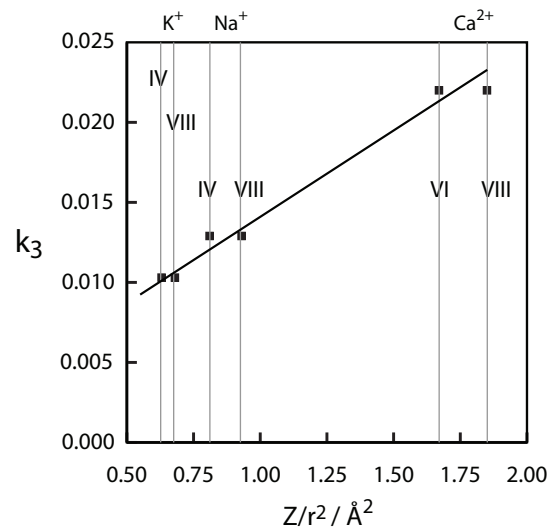
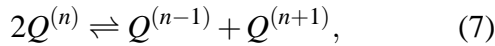


Figure 6: Disproportionation equilibrium constant,  $k_3$ , given in Eq (7), measured using  $^{29}\text{Si}$  2D MAF NMR as a function of network modifier cation potential, where  $Z$  is the charge of the coordinating cation and  $r$  is the radius of the cation.

with different  $\zeta$  and  $\eta$ , as observed by Maekawa et al. (1991),<sup>35</sup> could also affect measured concentrations, influencing the calculated potassium to silicon ratio, and interfere with the three site model used when fitting the 2D MAF dataset.

A popular model, used in understanding the energetics and thermodynamic mixing properties of silicate melts,<sup>36,37</sup> and suggested as part of a mechanism for alkali ion transport in alkali silicate glasses,<sup>38,39</sup> involves the disproportionation equilibria between  $Q^{(n)}$  species,



with the equilibrium constant at the glass transition temperature,

$$k_n = [Q^{(n+1)}][Q^{(n-1)}]/[Q^{(n)}]^2. \quad (8)$$

The equilibrium constant for this disproportionation reaction ranges from  $k_n = 0$  for a highly ordered (i.e. binary) distribution of silicate anionic species to  $k_3 = 0.375$ ,  $k_2 = 0.439$ , and  $k_1 = 0.311$  for a completely random distribution.<sup>40,41</sup> Using the  $Q^{(n)}$  populations obtained in this study we can calculate an equilibrium constant of  $k_3 = 0.0103 \pm 0.0008$  for this composition. This value is consistent with previous studies<sup>23,35,42</sup> which indicate that potassium silicate glasses have a highly ordered distribution of silicate anionic species. Comparing this value with  $k_3$  values obtained in our two previous 2D <sup>29</sup>Si MAF studies of  $2 \text{ Na}_2\text{O} \cdot 3 \text{ SiO}_2$ , and  $\text{CaO} \cdot \text{SiO}_2$  glass we observe a strong correlation between  $k_3$  and modifier cation potential, as shown in Figure 6. The trend is consistent with earlier conclusions that higher charged cations shift the disproportionation reaction of Eq. (7) to the right.<sup>34,43</sup> Even after taking into account the possibility of different modifier cation coordination numbers, indicated by roman numerals in Figure 6, the correlation still appears to be relatively linear.

## Summary

We have obtained and analyzed a 2D MAF spectrum of <sup>29</sup>Si enriched  $\text{K}_2\text{O} \cdot 2 \text{ SiO}_2$  glass, whose 1D MAS spectrum is completely unresolved. By exploiting differences in <sup>29</sup>Si anisotropic line-

shapes characteristic for each  $Q^{(n)}$  species we have obtained accurate and quantitative  $Q^{(n)}$  populations. Even though the spectral analysis was unconstrained by composition and charge balance, the  $Q^{(n)}$  populations obtained were found to be consistent with those constraints. These  $Q^{(n)}$  populations were used to calculate the equilibrium constant for the disproportionation reaction of  $Q^{(3)}$  occurring in the melt, and confirmed that a close to binary distribution of anionic species exists in the potassium disilicate glass. The observed  $k_3$  value is also consistent with the expected trend of increasing  $Q^{(n)}$  disproportionation with increasing network modifier cation strength. In fact, based on previous MAF studies of sodium and calcium silicate glasses it appears that this relationship may be close to linear. Finally, the nuclear shielding anisotropy observed for both  $Q^{(2)}$  and  $Q^{(3)}$  sites were found to be consistent with established trends in which the <sup>29</sup>Si nuclear anisotropic shielding increases linearly with decreasing silicon–non-bridging oxygen bond length, which, in turn, increases when the non-bridging oxygen is coordinated by a modifier cation of lower potential. Future studies of alkali and alkaline earth glasses will clarify observed trends in  $\zeta$  and the equilibrium constant as a function of cation potential. Better understanding of how these values change will provide insight into atomic structure and how the silicate network changes as various modifying cations are added.

**Acknowledgement** This material is based upon work supported in part by the National Science Foundation under Grant No. CHE 0616881. The authors thank Professor Jonathan Stebbins for helpful discussions.

## References

- (1) Cable, M. High Performance Glasses. In *High Performance Glasses*; Cable, M., Parker, J. M., Eds.; Chapman and Hall: New York, 1992; p 1.
- (2) Zarzycki, J. *Glasses and the Vitreous State*; Cambridge University Press: Cambridge, 1991.
- (3) Zhang, P.; Dunlap, C.; Florian, P.;

- Grandinetti, P. J.; Farnan, I.; Stebbins, J. F. *J. Non. Cryst. Solids* **1996**, *204*, 294–300.
- (4) Zhang, P.; Grandinetti, P. J.; Stebbins, J. F. *J. Phys. Chem. B* **1997**, *101*, 4004–4008.
- (5) Bax, A.; Szeverenyi, N. M.; Maciel, G. E. *J. Magn. Reson.* **1983**, *55*, 494.
- (6) Grandinetti, P. J.; Lee, Y. K.; Baltisberger, J. H.; Sun, B. Q.; Pines, A. *J. Magn. Reson. A* **1993**, *102*, 195.
- (7) Dixon, W. T. *J. Chem. Phys.* **1982**, *77*, 1800.
- (8) Antzutkin, O. N.; Shekar, S. C.; Levitt, M. H. *J. Magn. Reson. A* **1995**, *115*, 7–19.
- (9) Gan, Z. H. *J. Am. Chem. Soc.* **1992**, *114*, 8307–8309.
- (10) Hu, J. Z.; Alderman, D. W.; Ye, C. H.; Pugmire, R. J.; Grant, D. M. *J. Magn. Reson. A* **1993**, *105*, 82–87.
- (11) Chan, J. C. C.; Tycko, R. *J. Chem. Phys.* **2003**, *118*, 8378–8389.
- (12) Duer, M. J.; Elliot, S. R.; Gladden, L. F. *J. Non Cryst. Solids* **1995**, *189*, 107–117.
- (13) Fayon, F.; Bessada, C.; Douy, A.; Massiot, D. *J. Magn. Reson.* **1999**, *137*, 116–121.
- (14) Montagne, L.; Donzea, S.; Palavita, G.; Boivina, J. C.; Fayon, F.; Massiot, D.; Grimblot, J.; Gengembre, L. *J. Non-Cryst. Solids* **2001**, *293-295*, 74–80.
- (15) Slejko, F. F.; Petrini, R.; Forte, C.; Pedrazzi, G.; Pinzino, C.; D'Antonio, M. *J. Non. Cryst. Solids* **2003**, *323*, 54–67.
- (16) Sakellariou, D.; Jacquinet, J.-F.; Charpentier, T. *Chem. Phys. Lett.* **2005**, *411*, 171–174.
- (17) Sakellariou, D.; Charpentier, T. *Appl. Magn. Reson.* **2007**, *32*, 583–594.
- (18) Feike, M.; Jäger, C.; Spiess, H. W. *J. Non-Cryst. Solids* **1998**, *223*, 200–206.
- (19) Witter, R.; Hartmann, P.; Vogel, J.; Jäger, C. *Solid State NMR* **1998**, *13*, 189–200.
- (20) Glock, K.; Hirsch, O.; Rehak, P.; Thomas, B.; Jäger, C. *Journal of Non-Crystalline Solids* **1998**, *232-234*, 113–118.
- (21) Olivier, L.; Yuan, X.; Cormack, A. N.; Jäger, C. *J. Non-Cryst. Solids* **2001**, *293-295*, 53–66.
- (22) Fayon, F.; Saout, G. L.; Emsley, L.; Massiot, D. *Chem. Comm.* **2002**, 1702–1703.
- (23) Malfait, W. J.; Halter, W. E.; Morizet, Y.; Meier, B. H.; Verel, R. *Geochimica et Cosmochimica Acta* **2007**, *71*, 6002–6018.
- (24) Florian, P.; Fayon, F.; Massiot, D. *J. Phys. Chem. C* **2009**, *113*, 2562–2572.
- (25) Grimmer, A.-R.; Gechner, E. F.; Molgedey, G. *Chem. Phys. Lett.* **1981**, *77*, 331–335.
- (26) Grimmer, A.-R. *Chem. Phys. Lett.* **1985**, *119*, 416–420.
- (27) Stebbins, J. F. *Nature* **1987**, *330*, 465.
- (28) Hansen, M. R.; Jakobsen, H. J.; Skibsted, J. *Inorg. Chem.* **2003**, *42*, 2368–2377.
- (29) Eastman, M. A.; Grandinetti, P. J.; Lee, Y. K.; Pines, A. *J. Magn. Reson.* **1992**, *98*, 333–341.
- (30) Grandinetti, P. J.; Baltisberger, J. H.; Llor, A.; Lee, Y. K.; Werner, U.; Eastman, M. A.; Pines, A. *J. Magn. Reson. A* **1993**, *103*, 72–81.
- (31) Mehring, M. *High Resolution NMR Spectroscopy in Solids*; Springer-Verlag: Berlin, 1983; Vol. 11.
- (32) Harris, R. K.; Becker, E. D.; Menezes, S. M. C. D.; Granger, P.; Hoffman, R. E.; Zilm, K. W. *Inorg. Chem.* **2008**, *3*, 41–56.
- (33) Whittaker, E. J. W.; Muntus, R. *Geochim. Cosmochim. Acta* **1970**, *34*, 945–956.
- (34) Stebbins, J. F. *J. Non Cryst. Solids* **1988**, *106*, 359–369.

- hal-00468378, version 1 - 30 Mar 2010
- (35) Maekawa, H.; Maekawa, T.; Kawamura, K.; Yokokawa, T. *J. Non-Cryst. Solids* **1991**, *127*, 53–64.
- (36) Navrotsky, A. Energetics of Silicate Melts. In *Structure , Dynamics and Properties of Silicate Melts*; Stebbins, J. F., McMillan, P. F., Dingwell, D. B., Eds.; Mineralogical Society of America: Washington, DC, 1995; Vol. 32, pp 121–143.
- (37) Hess, P. C. Thermodynamic Mixing Properties and the Structure of Silicate Melts. In *Structure , Dynamics and Properties of Silicate Melts*; Stebbins, J. F., McMillan, P. F., Dingwell, D. B., Eds.; Mineralogical Society of America: Washington, DC, 1995; Vol. 32, pp 145–190.
- (38) Greaves, G. N.; Gurman, S. J.; Catlow, C. R. A.; Chadwick, A. V.; Houde-Walter, S.; Henderson, C. M. B.; Dobson, B. R. *Phil. Mag. A* **1991**, *64*, 1059–1072.
- (39) Ingram, M. D. *Phil. Mag. B* **1989**, *60*, 729.
- (40) Vessal, B.; Wright, A. C.; Hannon, A. C. *J. Non Cryst. Solids* **1996**, *196*, 233–238.
- (41) Lacy, E. D. *Phys. Chem. Glasses* **1965**, *6*, 171–180.
- (42) Zakaznova-Herzog, V. P.; Malfait, W. J.; Herzog, F.; Halter, W. E. *Journal of Non-Crystalline Solids* **2007**, *353*, 4015–4028.
- (43) Murdoch, J. B.; Stebbins, J. F.; Carmichael, I. S. E. *Am. Mineral.* **1985**, *70*, 332–343.